 doi:10.20944/preprints201808.0063.v1

*Article*

# Bizarreness of ferrite formation in ingot of 0Cr17Ni4Cu4Nb stainless steel

**Fei Han [1], Haicheng Yu [2], Jeffrey Dessau [3] and Xianghai Chen [3, *]**

[1] Special Material Institute of Inner Mongolia North Heavy Industry Group Corp LTD, Baotou, China 0140332; CNASXD@xuanda.com
[2] Xuanda Metal Research Institute, Xuanda Industrial Group China Co., Ltd, WenZhou China 325105; XDLAB@xuanda.com
[3] Biological anti corrosion program, United Biologics Inc. Oakville, Ontario, Canada L6H 3K4; jeff.dessau@ubio.ca
* Correspondence: daniel.chen@ubio.ca; Tel.: +1-416-276-1005

**Abstract:** Ferrite body is the origin of crack and corrosion initiation of steels. Distribution and density of ferrite in seven steel ingots were examined by light optical microscopy and computational modeling in the study to explore the correlation of ferrite formation to chemical composition and mushy zone temperature in ingot forming. The central segregation phenomenon in ferrite distribution was observed in all the examined steel specimens except 0Cr17Ni4Cu4Nb stainless steel. No significant difference was found in distribution and density of ferrite amongst zones of the surface, ½ radius and core in neither riser nor tail of 0Cr17Ni4Cu4Nb ingot. Additionally, fewer ferrite was found in 0Cr17Ni4Cu4Nb compared to other examined steels. The bizarreness of ferrite formation observed in 0Cr17Ni4Cu4Nb elicited a debate on the traditional concepts explicating ferrite formation. Considering the compelling advantage in the mechanical strength, plasticity and corrosion resistance, further investigation on the unusual ferrite forming occurrence in 0Cr17Ni4Cu4Nb would help develop steels with improved quality. In summary, we observed that ferrite formation was correlated to mushy zone temperature, Cr:Fe and Cu:Fe ratios. We originally assume that Fe, the major component of steel could play an unrecognized role via proportion to other chemical components in ferrite formation.

**Keywords:** ferrite formation; mushy zone temperature, liquidus and solidus temperature, ingot forming, 0Cr17Ni4Cu4Nb stainless steel

## 1. Introduction

Typical 0Crl7Ni4Cu4Nb stainless steel is characteristic of low carbon (C) and high chemical elements of chromium (Cr), nickel (Ni) and copper (Cu). The steel is of duplex ferrite-austenite microstructure, and excellent in corrosion resistance and mechanical stability [1]. It is widely used in aerospace, turbine blades, food industry, offshore platforms and synthetic fiber mold manufacturing. However, the thermal plasticity of 0Crl7Ni4Cu4Nb remains to be improved. Cracks often arise in ingot forming and thermal forging process, which limit the service life of 0Crl7Ni4Cu4Nb steel in practice.

The service life of duplex ferrite-austenite steel highly de pends on aging factors, such as ferrite formation, chemical composition, thermal history, corrosion, microstructure and texture [2]. Among those factors, ferrite formation plays an essential role in steel aging. Ferrite in a steel leads to the decrease in ductility, toughness and impacts corrosion resistance, thus damage and fracture of steel tissue, and consequently limits its service life [2]. Ferrite is a blend of iron(Fe) and one or more additional metallic elements, such as Cr, C, molybdenum (Mo), and other alloying elements and is commonly formed at high temperature in steel forming, thus it is also called high temperature ferrite. In steel tissue, ferrite is susceptible to thermal hardening that leads to local premature cracking. The

Preprints (www.preprints.org) | NOT PEER-REVIEWED | Posted: 3 August 2018 doi:10.20944/preprints201808.0063.v1



formed cracks eventually become cavities that lead to the final ductile fracture by cavity growth and fusion [3]. Therefore, controlling of ferrite formation is the key technique to improve the mechanical property and prolong the service life of a steel.

Ferrite in steel can be divided into equilibrium and non-equilibrium phase ferrite according to the mechanism of ferrite body formation [4]. Ferrite body in the equilibrium state is mainly determined by the chemical composition of the steel. The increase of ferrite element contents, such as Cr, Mo, vanadium (V) and Silicon (Si) in steel tissue, can promote the formation of ferrite. The ferrite body, once formed, is difficult to be removed by subsequent thermal treatment. The ferrite in non-equilibrium state is generally formed at high temperature, which indeed is part of the steel tissue not yet transited into austenite in supercooling processes. The ferrite formed in non-equilibrium state can be thermally eliminated in subsequent processes. Ferrite also appears at the time of solidification and heat processing. The temporally different ferrites are various in morphology and distribution.

Up to date, the role of Fe, the major chemical component of steel in ferrite formation seems ignored in the main stream of research. Moreover, fewer publication is available, being addressed on ferrite formation in 0Crl7Ni4Cu4Nb stainless steel. The current study intends to fill up the research gap by exploring ferrite formation in 0Crl7Ni4Cu4Nb steel to reveal the possible correlation of the ferrite formation to the steel's compelling advantages of mechanical stability and corrosion resistance.

## 2. Materials and Methods

*2.1 Computational modeling to predict ferrite forming in correlation with chemical composition and mushy zone temperature of a steel.*

The thermo-values are obtained by thermos-analytical methods with the generally used empirically based formulas and thermos-dynamical Computherm software. Computational chromium formula $E\delta F = E_{Cr} + E_T$ was taken as the base mathematic equation in this study, combining chemical composition and forging temperature [1] as key simulation parameters. ECr represents chemical components and $E_T$ denotes the temperature equivalents. The formula was applied to simulate shrinkage styles of steel forming process (Fig. 4 and 5). Based on the formula developed by Gryc [10] and combination of dynamic thermal measurement of the melting temperature of 0Cr17Ni4Cu4Nb steel, the liquidus temperature was calculated with the equation 2, that is

$$T_L = 2619 - K\cdot(\%C) - 8\cdot(\%Si) - 5\cdot(\%Mn) - 30\cdot(\%P) - 25\cdot(\%S) - 1.7\cdot(\%Al) - 5\cdot(\%Cu) - 1.5\cdot(\%Cr) - 4\cdot(\%Ni) - 2\cdot(\%V) - 1\cdot(\%W) - 1.7\cdot(\%Co) - 12{,}8\cdot(\%Zr) - 7\cdot(\%Nb) - 3\cdot(\%Ta) - 14\cdot(\%Ti) - 14\cdot(\%As) - 10\cdot(\%Sn) - 1.59\cdot(\%Cr) + 0.007\cdot(\%Cr)2 \quad (2)\ [11]$$

where the K coefficient varies with respect to different contents of carbon: C > 2 %; K = 65

C < 2%; K = 88.

The solidus was determined by equation 3, that is

$$Ts = 2619 - [415.5(\%C) + 12.3(\%Si) + 6.8\ (\%Mn) + 124.5(\%P) + 183.9(\%S) + 4.3(\%Ni) + 1.4(\%Cr) + 4.1(\%Al)] \quad (3)\ [11]$$

The chemical composition of 0Cr17Ni4Cu4Nb, listed in table 1 below, are used as parameters to compute liduidus and solidus values.

Table 1. 0Cr17Ni4Cu4Nb internal control chemical composition (%)

| *C* | *Si* | *Mn* | *S* | *P* | *Cr* |
|---|---|---|---|---|---|
| ⩽ | ⩽ | ⩽ | ⩽ | ⩽ | 15.00 |
| 0.055 | 1.00 | 0.50 | 0.025 | 0.030 | 16.00 |
| Ni | Cu | Al | Ti | N | Nb+Ta |
| 3.80 | 3.00 | ⩽ | ⩽ | ⩽ | 0.15 |
| 4.50 | 3.70 | 0.050 | 0.050 | 0.050 | 0.35 |

 doi:10.20944/preprints201808.0063.v1



*2.2 Microscopic examination of ferrite morphology, distribution and density of ferrite in different zones and positions of steel ingot.*

The specimens made of stainless steel were Ø10 mm polished cylinders with a length of 30 mm. Microstructures of steel sample tissues were examined by light optical microscopy. Slices of steel sample were repeatedly polished to 0.1mm in thickness, then corroded with ferric chloride and hydrochloric acid solution prior to quantify ferrite content in the slices under microscope. The gold phase method was used to determine the region of interest by superimposing the mesh on the image under the metallographic microscope. The number of targets or the total number of test points were divided by the number of grids and the average value was taken as the result. The final results were the average value of the N monitoring field.

## 3. Results

*3.1. Ferrite formation in steel was associated with mushy zone temperature.*

The intrinsic liquidus and solidus temperatures of seven steels different in chemical composition were measured and the difference between liquidus and solidus, named mushy zone temperature ($T_L$-Ts), were calculated as shown in the Table 2 and Figure 1. The mushy zone temperature gradually decreased in the order of stainless steel 0Crl7Ni4Cu4Nb >P91>H13>42CrMo in correlation with the decrease of Cr and Cu content, while mushy zone is decreased in correspondence to the increase of C content in the all examined steels. Notably, there is an observable difference in mushy zone temperature between P91 and H13 though Fe contents in each of the stainless steels were almost same (89 vs 89.995%), indicating Fe could play an unrecognized role to determine the mushy zone temperature of a steel. Further analyses found that mushy zone temperatures of stainless steels were closely correlated to Cr:Fe and Cu:Fe ratios (Table 2, Fig. 2 & 3). The higher both the ratios were, the higher the mushy zone temperature of a stainless steel in trend. The observation implied that ratios of certain chemical components, such as Cr:Fe and Cu:Fe ratios play a more important role to determine the mushy zone temperature of a stainless steel. The trends were not observed in carbon steels.

Table 2. Correlation of mushy zone to chemical composition of steels

| | C | Si | Mn | V | Cr | Mo | Ai | N | Nb | Ni | Cu | P | S | Fe | L* | S* | $T_L$-$T_S$ |
|---|---|---|---|---|---|---|---|---|---|---|---|---|---|---|---|---|---|
| **P91** | 0.08 | 0.2 | 0.3 | 0.18 | 8 | 0.9 | 0 | 0.03 | 0.06 | 0 | 1.25 | 0 | 0 | 89 | 1509 | 1326 | **183** |
| **H13** | 0.405 | 1 | 0.35 | 1 | 5.125 | 1.425 | 0 | 0 | 0 | 0 | 0.7 | 0 | 0 | 89.995 | 1472 | 1345 | **127** |
| **42CrMo** | 0.42 | 0.25 | 0.7 | 0.05 | 1 | 0.17 | 0.01 | 0 | 0 | 0 | 0 | 0 | 0 | 97.4 | 1493 | 1440 | **53** |
| **Low C** | 0.08 | 0.08 | 0.31 | 0 | 0.45 | 0 | 0 | 0 | 0 | 0 | 0 | 0.03 | 0.05 | 99 | 1526 | 1446 | **80** |
| **Medium C** | 0.23 | 0.11 | 0.63 | 0 | 0 | 0 | 0 | 0 | 0 | 0.07 | 0 | 0.034 | 0.034 | 98.892 | 1516 | 1430 | **86** |
| **High C** | 0.8 | 0.13 | 0.32 | 0 | 0.11 | 0 | 0 | 0 | 0 | 0.13 | 0 | 0.009 | 0.009 | 98.492 | 1473 | 1370 | **103** |
| **0Cr17*** | 0.55 | 1 | 0.5 | 0 | 16 | 0.4 | 0.05 | 0.05 | 0.3 | 4.2 | 3.7 | 0.03 | 0.02 | 73.2 | 1427 | 1205 | **222** |

Note: 0Cr17* - 0Crl7Ni4Cu4Nb; L* - liquidum; S* - solidum; $T_L$-$T_S$: L* - S*

The simulated liquidum and solidum temperatures of 0Crl7Ni4Cu4Nb were detrermined by the formula 2 and 3 as listed in Material and Methods. The mushy zone temperature of 0Crl7Ni4Cu4Nb is higher than that of all other examined steels.

Preprints (www.preprints.org) | NOT PEER-REVIEWED | Posted: 3 August 2018 doi:10.20944/preprints201808.0063.v1



Figure 1. The simulated liquidum and solidum temperatures of 0Crl7Ni4Cu4Nb

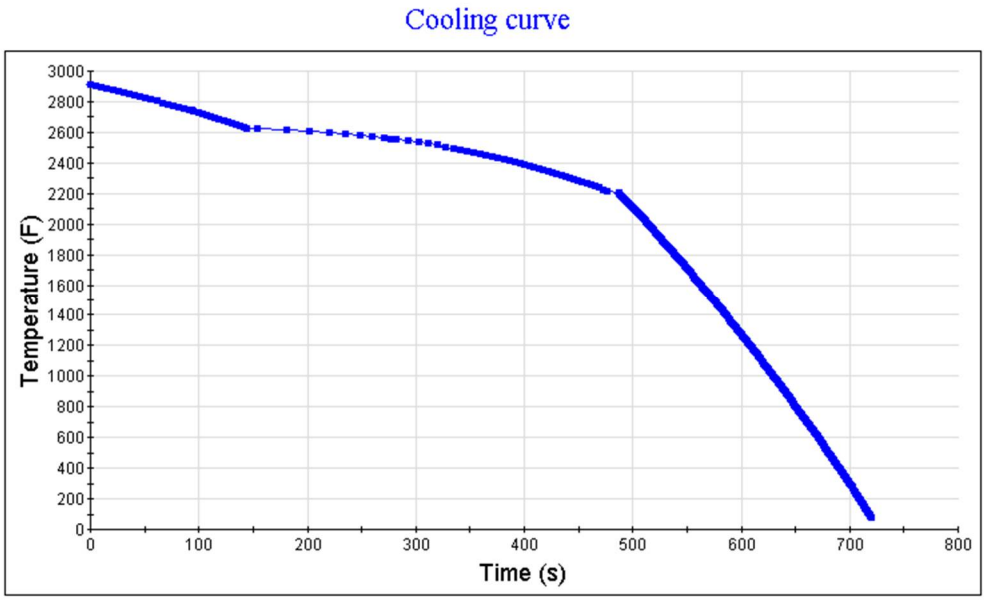


As shown in Table 3, Cr:Fe and Cu:Fe decreased in correlation to the decrease of mushy zone temperature in correlation coefficient between the dependent variables of mushy zone and Cr:Fe and Cu:Fe ratios.

Table 3 Correlation of mushy zone to Cr:Fe, Cu:Fe and Cr:C ratio

| | Cr:Fe | Cu:Fe | Cr:C | Cu:C | $T_L$-$T_S$ |
|---|---|---|---|---|---|
| **0Cr17** | 0.219 | 0.051 | 29 | 6.73 | 222 |
| **P91** | 0.090 | 0.014 | 100.000 | 15.625 | 183 |
| **H13** | 0.057 | 0.008 | 12.654 | 1.728 | 127 |
| **42CrMo** | 0.010 | 0.000 | 2.381 | 0.000 | 53 |

Further analysis found that as shown in Figure 2, the ratio of Cr:Fe is closely correlated to mushy zone temperature, based on that the coefficient of determination - squared correlation coefficient $R^2$ equals as high as 93.91%. The computational outcome verifies the hypotheses that Cr:Fe ratio, rather the absolute Cr content could play a more important role to determine mushy zone temperature of a stainless steel. A steel with higher Cr:Fe ratio could have a relative higher mushy zone temperature.

Figure 2. Correlation of Cr:Fe to mushy zone temperature

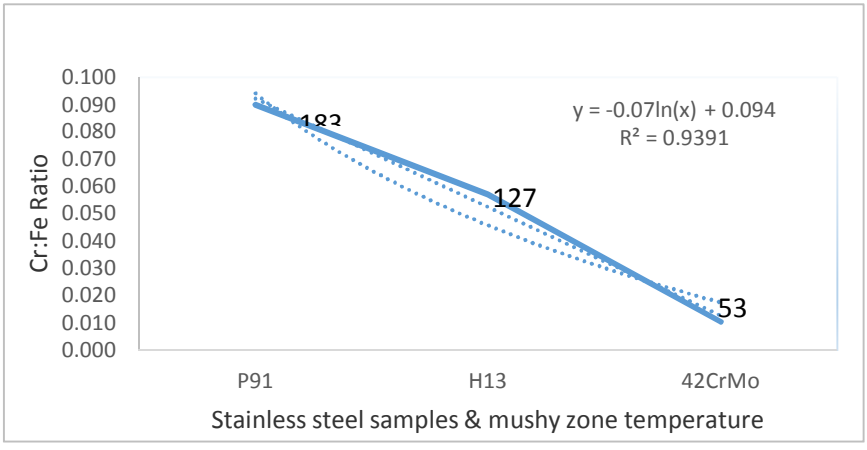

Preprints (www.preprints.org) | NOT PEER-REVIEWED | Posted: 3 August 2018 doi:10.20944/preprints201808.0063.v1



As shown in Figure 3. mushy zone temperature was also correlated to Cu:Fe ratio. As squared correlation coefficient $R^2$ is as high as 97.19%, the computational model could provide a measure of how well mushy zone temperature are replicated, based on Cu:Fe proportion. A steel with higher Cu:Fe ratio could have higher mushy zone temperature potential.

Figure 3. Correlation of Cu:Fe to mushy zone temperature

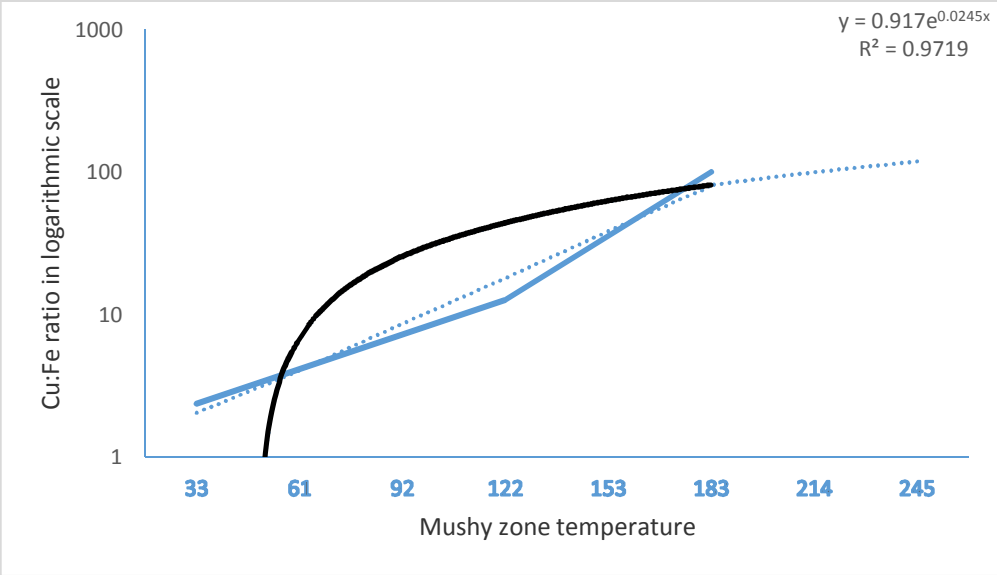


*3.2 Ferrite density and distribution in steel were correlated with mushy zone temperature*

Shrinkage styles of steel ingot forming were simulated with different mushy zone temperature using Anycasting software. As shown in Figure 4, P91 stainless steel with higher mushy zone temperature was shrunk in "I" style and resulted in a deep ferrite band (labeled as "d") in the core region from riser to tail of the ingot, while H13, the stainless steel with low mushy zone temperature, was shrunk in "Y" panache and molded a superficial ferrite zone in the central region of riser, not in the tail portion. Almost no ferrite zone was formed in 42CrMo, the stainless steel with the lowest mushy zone temperature.

Figure 4. Simulation of style of ferrite formation in stainless steel ingots with different mushy zone temperatures

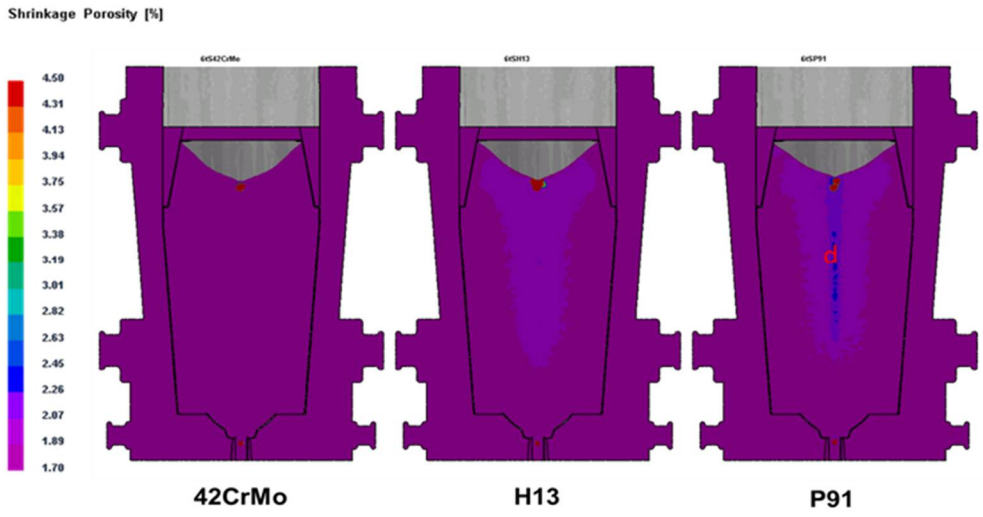

Preprints (www.preprints.org) | NOT PEER-REVIEWED | Posted: 3 August 2018 doi:10.20944/preprints201808.0063.v1



Ferrite formation correlating to mushy zone temperature was also demonstrated in high carbon steel that is with high mushy zone temperature as shown in Figure 5. A style between "Y" and "I" was developed in high carbon steel, formed a deep and wide ferrite band in the central region. No apparent ferrite bands were developed in low carbon steel that was with low mushy zone temperature.

Figure 5. Simulation of style of ferrite formation in carbon steels ingots with different mushy zone temperatures

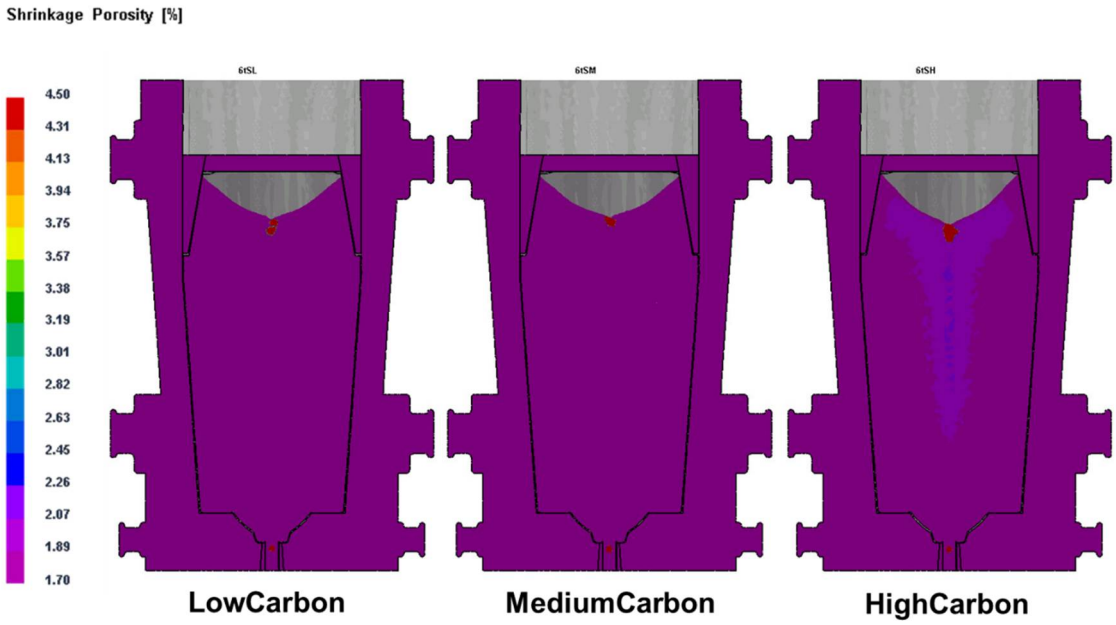


*3.3 Distributions of ferrite in all the examined stainless and carbon steel ingots were complied with the simulated shrinkage style and the central segregation concept, except 0Crl7Ni4Cu4Nb stainless steel. Fewer ferrite was found in 0Crl7Ni4Cu4Nb.*

Specimens were collected from the seven steel samples for microstructural characterization by light optical microscopy (LOM). The specimens were mounted in planar view to examine the solidification ferrites, which intersected the sample surface. All specimens were polished to slices in 0.1-mm thickness in hydrochloric acid solution. Samples taken from the surface region, ½ radius zone and core region in the riser and tail of stainless steel ingots were examined under LOM metallurgic microscope.

Figure 6. Distribution, density and morphology of ferrite in riser of steel ingots

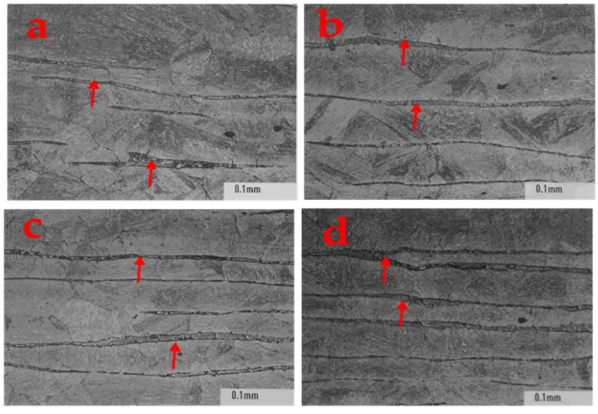

Preprints (www.preprints.org) | NOT PEER-REVIEWED | Posted: 3 August 2018 doi:10.20944/preprints201808.0063.v1



As shown in Figure 6, photo "a" represented the steel tissue in surface zone of ingot riser. Obviously, ferrite content (uneven coarse black banded strips that red arrow lines point on) in the zone is much less than that in the ½ radius zone (Photo "b" and "c") and the core region (Photo "d") of the ingot. Ferrites in the central region (the labeled "d" region of P91 on Figure 4 as an example) presented as continuous coarse black banded strips with the increased density. The observed surface area was adjusted to the standard of metallographic determination of area content of alpha phase in GB/T13305-2008 austenitic stainless steel. The adjusted ferrite contents in five different fields were averaged and summarized.

Using the same method, the distribution and density of ferrite at surface and the vertical zones were prudently examined in riser and tail of three 0Cr17Ni4Cu4Nb ingots. Notably, as shown in Table 3, the density of ferrite in all the examined radius regions in riser and tail was less than 5%, showing no statistically significant difference relevant to the distribution in the tested 0Cr17Ni4Cu4Nb steel samples.

Table 4. Ferrite content detected in 0Cr17Ni4Cu4Nb steel material

| *ingot number* | *position* | *part* | *ferrite %* | *position* | *part* | *ferrite %* |
|---|---|---|---|---|---|---|
| 15121 | riser | The outer wall | 4 | Ingot tail | The outer wall | 3 |
| | | 1/2 radius | 3 | | 1/2 radius | 2 |
| | | core | 1 | | core | 5 |
| 25266 | riser | The outer wall | 5 | Ingot tail | The outer wall | 4 |
| | | 1/2 radius | 3 | | 1/2 radius | 3 |
| | | core | 4 | | core | 4 |
| 25269 | riser | The outer wall | 4 | Ingot tail | The outer wall | 4 |
| | | 1/2 radius | 5 | | 1/2 radius | 4 |
| | | core | 5 | | core | 5 |
| GB/T8732 | – | – | ⩽10 | – | – | ⩽10 |

### *3.4 The simulated ferrite formation was in accordance with the experimental results that mushy zone temperature governs ferrite formation in steel ingot*

As shown in Figure 7, simulated with Formula 1, the vertical section for Fe-C-Cr phase diagram with 0.05%C shifted to the biphasic zone of high temperature ferrite and austenite when Cr content was set up at a high range as 17% and a high heating temperature at 1200 $^{0}$C. The simulation result was complied with the established conclusion that high Cr (relevant to higher Cr:C and Cr:Fe ratios) and temperature promote ferrite formation.

Ferrite formation in corresponding to temperature was estimated by Formula (1). That is

 doi:10.20944/preprints201808.0063.v1



$E_T$=[T（℃）-1150]/80 （1）

Figure 7. Vertical section diagram of Fe-C-Cr phase diagram with 0.05%C

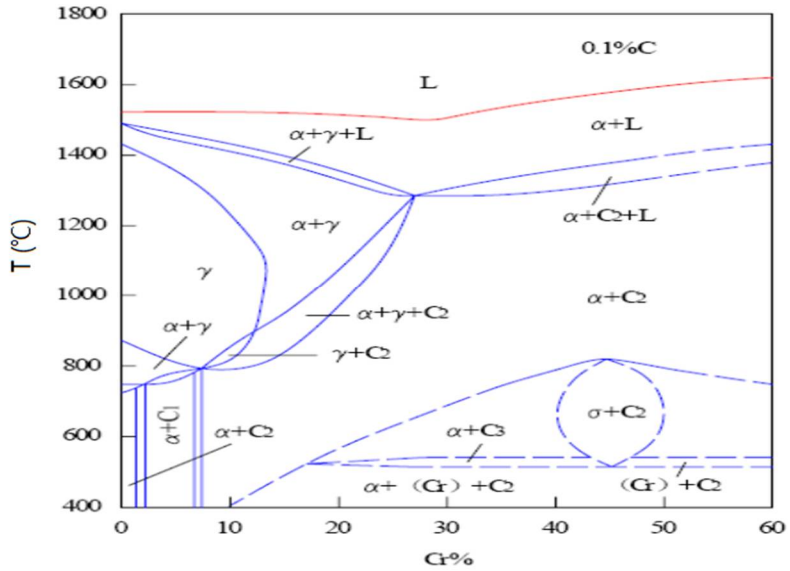


## 4. Discussion

Ferrite is the origin of crack initiation and corrosion commencement of steels [5]. Theoretically, minimizing of ferrite formation and thickening of ferrite-free surface zone are potential measures to improve the mechanical stability and corrosion resistance of a steel. Thus, it is necessary to understand the mechanism of ferrite formation and distribution in the process of steel forming.

The current study investigated the correlation of ferrite formation to chemical composition and mushy zone temperature (the difference between solidus and liquidus temperatures $T_L$-$T_S$). Ferrite is generally formed at high temperature [5]. At the beginning of ingot forming, the L to Delta transformation occurs first, then followed by the peritectic transformation to form austenite Gamma. Ferrite is often nucleated and grown up in the material when the processing temperature reaches Delta and Gamma phase or Delta single-phase region. It could be retained in the tissue if the formed ferrite was not completely transformed into austenite gamma when cooling [13]. As shown in Figure 6, the morphology, density and distribution pattern of ferrite in stainless steel P91 are different in various zones away from surface. More ferrite showing as continuous densified banded strips were observed in the core region than in regions close to surface of ingot. This phenomenon could be attributable to the central segregation propensity of ferrite forming elements in the solidification process in addition to that the temperature in core region is higher due to relatively slower heat exchange compared to the region close to surface.

Previous studies concluded that solidus and liquidus temperatures of a stainless steel were determined by its chemical composition [5, 13]. Proper forging temperature relevant to solidus and liquidus temperatures can minimize the secondary ferrite formation and extend ferrite-free surface zone during forging process. Several computational models have been developed for simulation of ferrite formation in correlation to temperature in stainless steel. Formula (1) $E_T$=[T（℃）-1150]/80 is high in reliability to predict ferrite formation tendency [5, 6, 13]. The reliability of Formula (1) was validated with experimental data from several studies testing various types of steel as shown in Figure 6. Based on the formula, optimal temperatures for thermal treatment to various steels have been established. For example, the forging temperatures of stainless steel and heat-resistant steel are generally set up below 1180 $^0$C [6], the initial forging and final forging temperatures of 0Cr13, 1Cr13, 2Cr13 and 3Cr13 are 1150 $^0$C and 850 $^0$C, respectively; the initial forging and final forging temperatures of 1Cr18Ni9Ti are 1180 $^0$C and 850 $^0$C; and the initial forging and final forging temperatures of 2Cr3WMoV are 1150 $^0$C and 800 $^0$C. Formula 1 was further validated with C

 doi:10.20944/preprints201808.0063.v1



controlled steel. As shown in Figure 7, simulated with Formula 1, the vertical section for Fe-C-Cr phase diagram of 0.05%C shifted to the biphasic zone of high temperature ferrite and austenite when Cr content was set up in a high range as 17% at a high heating temperature at 1200 $^0$C. The simulation result was complied with the established conclusion that high Cr and temperature promote ferrite formation, in return, the result verified the reliability of formula 1 and 2 in prediction of ferrite formation.

Computational programs have been also used to predict ferrite formation in high carbon steel precipitation hardening process [7, 8]. Those programs took elements referring to chemical composition as simulating parameters, which can predict tendency, but not quantitatively estimates of ferrite formation. The chromium formula $E\delta F = E_{Cr} + E_T$ was up-graded to Equation (1) and (2) in considering with numerous ferrite formation affecting factors of chemical composition vs mushy zone and forging temperatures. The effect of each element of chemical composition on ferrite formation phase was expressed in chromium equivalence. The chemical composition elements (Cr, Mo, W, V, Nb, Al, Si) were considered as factors favorable to ferrite formation, while the austenite forming elements (C, N, Mn, Ni, Cu) were regarded as inhibitors to the appearance of ferrite. According to the chemical composition of 0Crl7Ni4Cu4Nb steel, Cr equivalent $E_{Cr}$ formula (2) as shown below was established corresponding to the effective index of each chemical element.

$$E_{Cr} = Cr\text{-}40C\text{-}2Mn\text{-}4Ni\text{+}6Si\text{+}4Mo\text{+}11V\text{-}30N\text{+}1.5W \quad (2)\ [9]$$

$E_{Cr}$ in Formula (2) was regarded as the simulating index of chemical composition controlling ferrite formation in tapping steel. C, N and V, as seen in the formula, have greater impacts on ferrite formation, followed by Si, Mo, Ni, Mn. Theoretically, ferrite could be minimized, or even totally avoided in steel tissue by an attentive control of chemical components within appropriate ranges, based on Formula (2).

Ferrite could be also formed during the forging process for implementing an inappropriate high temperature in thermal treatment, or an overtime heat preservation procedure [1, 2]. Ferrite formation in corresponding to temperature was estimated by Formula (1).

The observation of the current study is aligned with the previous reported results that ferrite formation in stainless steels is different in those with dissimilar compositions [2, 3, 5, 12]. In the study, we found that ferrite formation in a steel ingot was highly relevant to the mushy zone temperature. The mushy zone temperature is a critical parameter for proper adjustment of models (physical or numerical) or in the final stage of applied research of the real process. It is significantly affecting the final quality of the as-cast steel (billets or ingots). More ferrites were observed in as-cast steels with high Cr and C. We realized that previous studies could have ignored the role of Fe, the major chemical content in ferrite formation. Based on our observation, we assume that ratios of Cr:Fe, Cu:Fe and Cr:C, rather arbitrary Cr, Fe and C quantities, could be more relevant to ferrite formation in stainless steel as shown in Figure 2, 3, 4 and 5. Notably, as presented in Table 4, both the distribution pattern and density of ferrite in 0Cr17Ni4Cu4Nb ingot risers and tails were deviated from the phenomenon of central segregation propensity observed in all other examined steels in the study. Ferrite content was much lower than that in standard reference steel GB/T8732 although Cr concentration was as high as 16% (Table 1) and forging temperature reached up to 1300 C. Inexplicably, fewer ferrite presented in the steel tissue though its mushy zone temperature was as high as 222 $^0$C. Supposedly, 0Cr17Ni4Cu4Nb steel was of more ferrite contents because its mushy zone temperature was higher than that of all other tested steels. A few questions were arisen from the observed bizarreness of ferrite formation in 0Cr17Ni4Cu4Nb steel. Could there be any critical threshold temperature of mushy zone that control ferrite forming? Could behaviors of ferrite forming elements change in manipulating ferrite formation at temperatures beyond the critical threshold? Since the effect of Ni, Cu relevant to Cr, C and Fe on ferrite formation have not been experimentally proved yet, further studies will be required.

In responding to the inevitable ferrite formation in steels, strategies to improve steel's quality should include minimizing ferrite content in steel forming process and exploiting the existing ferrite in steel tissue. The current main stream of study is mainly focused on the control of ferrite forming in steel process. As an alternative approach to extend the service life of a steel, more attentions have

 doi:10.20944/preprints201808.0063.v1



been attracted to exploit the existing ferrite in steel tissue. A biological metal coating technology developed by United Biologics Inc. in Canada is a typical such example taking advantage of the existing ferrite to improve steel's corrosion resistance and mechanical stability (publication and patent in process).

## 5. Conclusions

The current study is the first to draw an attention on the effect of Fe – the key component of steel on ferrite formation in steel. As observed in the current study, ratios of Cr:Fe, Cu:Fe and Cr:C are more relevant to mushy zone temperature of steel. While mushy zone temperature is closely correlated to ferrite formation. The larger the difference between the liquidus and solidus temperature, the greater the propensity of ferrite formation. In the majority of the examined steels in the study, ferrites distributed in the regions away from surface zone, and gathered in the core region of steel ingot due to the tendency of central segregation property of ferrite forming elements and relatively higher temperature in the central zone during ingot forming process. However, we found that ferrite formation in 0Cr17Ni4Cu4Nb stainless steel was deviated from the general rule of ferrite formation that was in comply with the majority of examined steels in the study. Fewer ferrite randomly distributed in various zones of 0Cr17Ni4Cu4Nb steel tissue though it has a high mushy zone temperature. The observation could be associated with relative higher Cr:Fe and Cu:Fe ratios, mushy zone temperature, and higher contents of ferrite inhibitory elements Ni and Cu in the steel. Though the observation remains inexplicable, a few inferences can be drawn from the study. (1). Fe, the major component of steel could play an unrecognized role in ferrite formation through its proportion to other chemical components, such as Cr, Cu and C in stainless steels; (2). Mushy zone temperature was an important intrinsic factor affecting ferrite formation; (3). Distribution of ferrite in steel tissue generally follows the central segregation phenomenon in majority of steels; (4). The advantages of 0Crl7Ni4Cu4Nb in corrosion resistance and mechanical stability could be arisen from the fact that fewer ferrite content and randomly scattered in steel tissue. This distribution pattern could be attributable to a relative low chance for scattered ferrite bodies to merge together, thus improved the mechanical stability and corrosion resistance of the steel. Alternatively, it could further improve steel's service time by exploiting the remaining ferrite in steel tissue.

**Author Contributions:** Conceptualization, Fei Han, Haicheng Yu and Xianghai Chen; Methodology, Fei Han and Xianghai Chen.; Software, Fei Han and Haicheng Yu.; Validation, Haicheng Yu. Jeffrey Dessau and Xianghai Chen.; Formal Analysis, Fei Han, Jeffrey Dessau and Xianghai Chen.; Investigation, Xianghai Chen Fei Han, Haicheng Yu; Resources, Xuanda Metal Research Institute.; Data Curation, Xuanda Metal Research Institute.; Writing-Original Draft Preparation, Fei Han.; Writing-Review & Editing, Xianghai Chen and Jeffrey Dessau; Visualization, Jeffrey Dessau.; Supervision, Xianghai Chen.; Project Administration, Haicheng Yu and Jeffrey Dessau; Funding Acquisition, Xuanda Metal Research Institute.

**Funding:** This research received no external funding

**Acknowledgments:** We would acknowledge the imaging lab at Xuanda Metal Research Institute for their kind support in steel specimen preparation.

**Conflicts of Interest:** The authors declare no conflict of interest. The funders had no role in the design of the study; in the collection, analyses, or interpretation of data; in the writing of the manuscript, and in the decision to publish the results.

Preprints (www.preprints.org) | NOT PEER-REVIEWED | Posted: 3 August 2018 doi:10.20944/preprints201808.0063.v1



## Appendix A

Figures

Figure 1. Liquidum and solidum temperatures of 0Crl7Ni4Cu4Nb

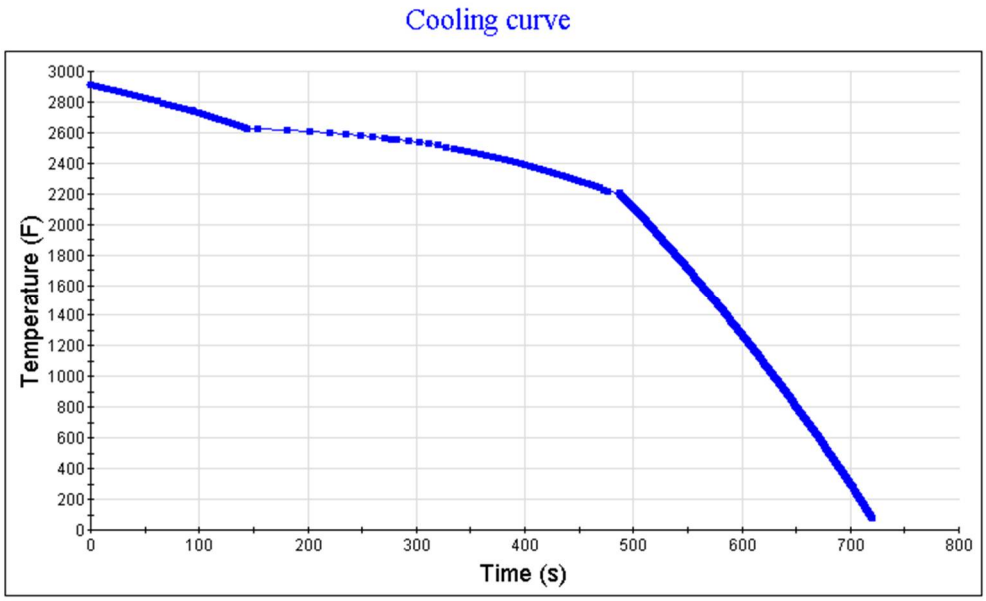


Figure 2. Correlation of Cr:Fe to mushy zone temperature

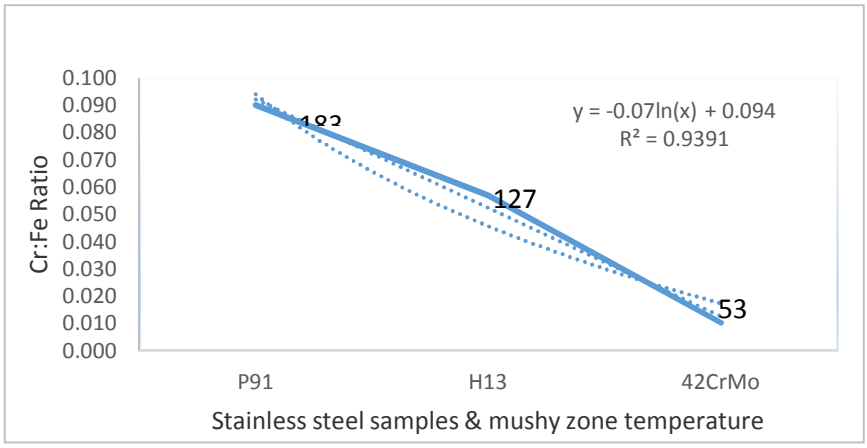

Preprints (www.preprints.org) | NOT PEER-REVIEWED | Posted: 3 August 2018 doi:10.20944/preprints201808.0063.v1



Figure 3. Correlation of Cu:Fe to mushy zone temperature

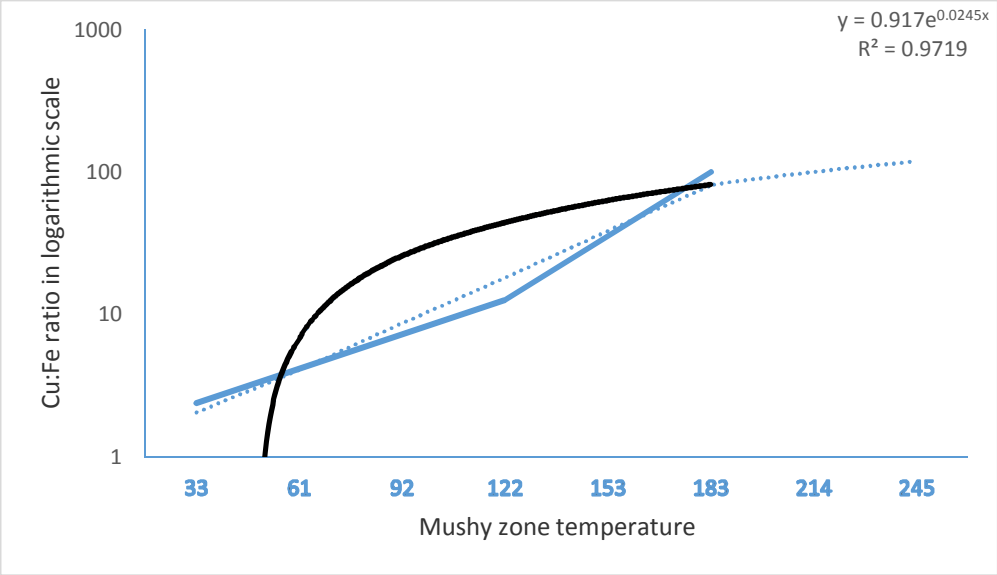


Figure 4. Simulation of style of ferrite formation in stainless steel ingots with different mushy zone temperatures

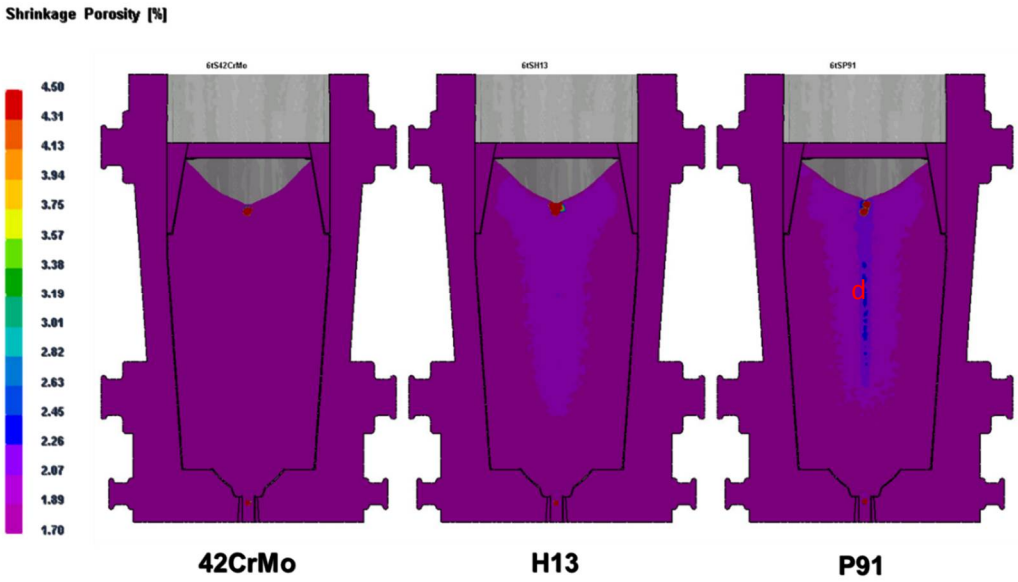

 doi:10.20944/preprints201808.0063.v1



Figure 5. Simulation of style of ferrite formation in carbon steels ingots with different mushy zone temperatures

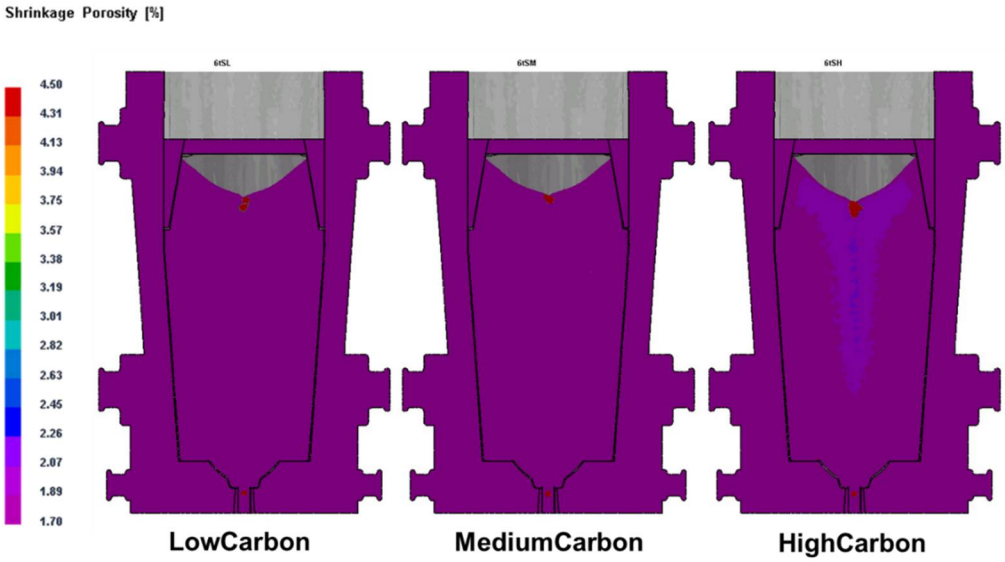


Figure 6. Distribution, density and morphology of ferrite in riser of steel ingots

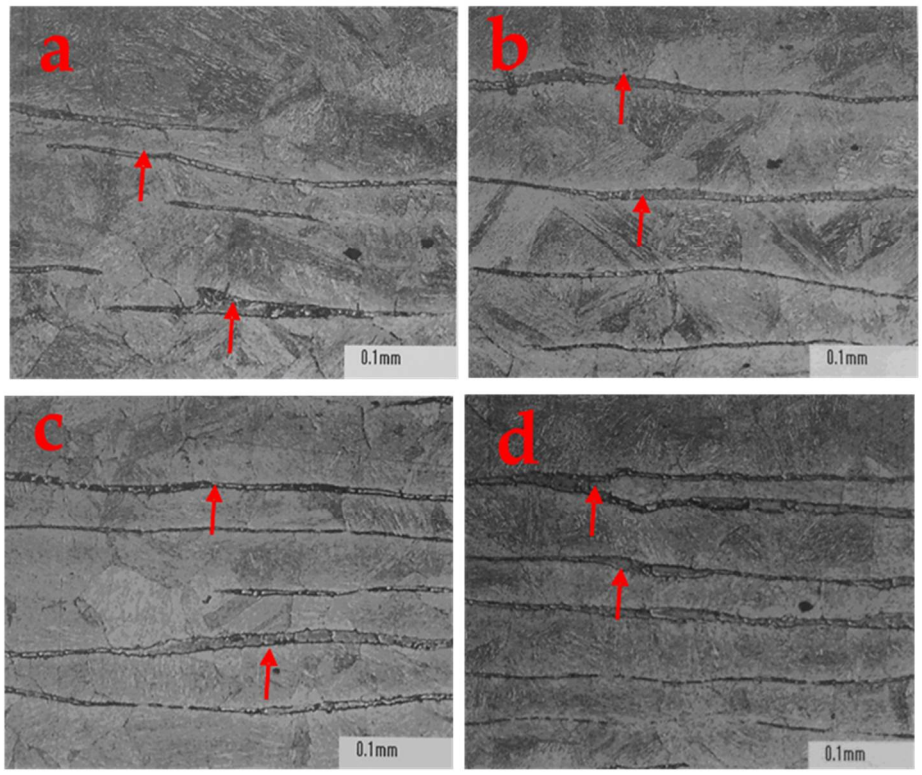

Preprints (www.preprints.org) | NOT PEER-REVIEWED | Posted: 3 August 2018 doi:10.20944/preprints201808.0063.v1



Figure 7. Vertical section diagram of Fe-C-Cr phase diagram of steel with 0.05%C

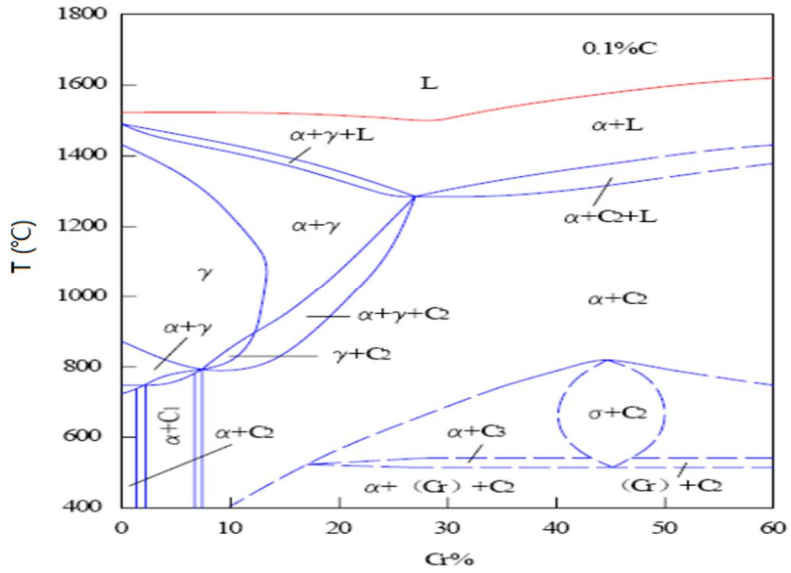


Tables

Table 1. 0Cr17Ni4Cu4Nb internal control chemical composition (%)

| *C* | *Si* | *Mn* | *S* | *P* | *Cr* |
|---|---|---|---|---|---|
| ≤ | ≤ | ≤ | ≤ | ≤ | 15.00 |
| 0.055 | 1.00 | 0.50 | 0.025 | 0.030 | 16.00 |
| Ni | Cu | Al | Ti | N | Nb+Ta |
| 3.80 | 3.00 | ≤ | ≤ | ≤ | 0.15 |
| 4.50 | 3.70 | 0.050 | 0.050 | 0.050 | 0.35 |

Table 2. Correlation of mushy zone to chemical composition of steels

| | C | Si | Mn | V | Cr | Mo | Ai | N | Nb | Ni | Cu | P | S | Fe | L* | S* | $T_L$-$T_S$ |
|---|---|---|---|---|---|---|---|---|---|---|---|---|---|---|---|---|---|
| **P91** | 0.08 | 0.2 | 0.3 | 0.18 | 8 | 0.9 | 0 | 0.03 | 0.06 | 0 | 1.25 | 0 | 0 | 89 | 1509 | 1326 | 183 |
| **H13** | 0.405 | 1 | 0.35 | 1 | 5.125 | 1.425 | 0 | 0 | 0 | 0 | 0.7 | 0 | 0 | 89.995 | 1472 | 1345 | 127 |
| **42CrMo** | 0.42 | 0.25 | 0.7 | 0.05 | 1 | 0.17 | 0.01 | 0 | 0 | 0 | 0 | 0 | 0 | 97.4 | 1493 | 1440 | 53 |
| **Low C** | 0.08 | 0.08 | 0.31 | 0 | 0.45 | 0 | 0 | 0 | 0 | 0 | 0 | 0.03 | 0.05 | 99 | 1526 | 1446 | 80 |
| **Medium C** | 0.23 | 0.11 | 0.63 | 0 | 0 | 0 | 0 | 0 | 0 | 0.07 | 0 | 0.034 | 0.034 | 98.892 | 1516 | 1430 | 86 |
| **High C** | 0.8 | 0.13 | 0.32 | 0 | 0.11 | 0 | 0 | 0 | 0 | 0.13 | 0 | 0.009 | 0.009 | 98.492 | 1473 | 1370 | 103 |
| **0Cr17*** | 0.55 | 1 | 0.5 | 0 | 16 | 0.4 | 0.05 | 0.05 | 0.3 | 4.2 | 3.7 | 0.03 | 0.02 | 73.2 | 1427 | 1205 | 222 |

Table 3. Correlation of mushy zone to Cr:Fe, Cu:Fe and Cr:C ratio

| | Cr:Fe | Cu:Fe | Cr:C | Cu:C | $T_L$-$T_S$ |
|---|---|---|---|---|---|
| **0Cr17** | 0.219 | 0.051 | 29 | 6.73 | 222 |
| **P91** | 0.090 | 0.014 | 100.000 | 15.625 | 183 |
| **H13** | 0.057 | 0.008 | 12.654 | 1.728 | 127 |
| **42CrMo** | 0.010 | 0.000 | 2.381 | 0.000 | 53 |

 doi:10.20944/preprints201808.0063.v1



Table 4. Ferrite content detected in 0Cr17Ni4Cu4Nb steel material

| *ingot number* | *position* | *part* | *ferrite %* | *position* | *part* | *ferrite %* |
|---|---|---|---|---|---|---|
| 15121 | riser | The outer wall | 4 | Ingot tail | The outer wall | 3 |
| | | 1/2 radius | 3 | | 1/2 radius | 2 |
| | | core | 1 | | core | 5 |
| 25266 | riser | The outer wall | 5 | Ingot tail | The outer wall | 4 |
| | | 1/2 radius | 3 | | 1/2 radius | 3 |
| | | core | 4 | | core | 4 |
| 25269 | riser | The outer wall | 4 | Ingot tail | The outer wall | 4 |
| | | 1/2 radius | 5 | | 1/2 radius | 4 |
| | | core | 5 | | core | 5 |
| GB/T8732 | – | – | ≤10 | – | – | ≤10 |

 doi:10.20944/preprints201808.0063.v1



## Appendix B

Figures



Tables



## References

1. M. R. Tavakoli Shoushtari, M. H. Moayed, and A. Davoodi, "Post-weld heat treatment influence on galvanic corrosion of GTAW of 17-4PH stainless steel in 3.5% NaCl," Corrosion Engineering Science and Technology, vol. 46, no. 4, pp. 415–424, 2011.
2. O. Hassan, I. brahima Ibrahim, S. IbrahimbTarek, A. Fouad Khalifa, Effect of Aging on the Toughness of Austenitic and Duplex Stainless Steel Weldments. Journal of Materials Science & Technology Volume 26, Issue 9, 2010, Pages 810-816.
3. P. Joly, R. Cozar, A. Pineau. Effect of crystallographic orientation of austenite on the formation of cleavage cracks in ferrite in an aged duplex stainless steel, Scripta Metallurgica et Materialia Volume 24, Issue 12, December 1990, Pages 2235-2240.
4. G. P. Krielaart, J. Sietsma, S. der Zwaag Ferrite formation in Fe-C alloys during austenite decomposition under non-equilibrium interface conditions Materials Science and Engineering: A Volume 237, Issue 2, September 1997, Pages 216-223.
5. B. G. Thomas, J.K. B1imacombe, and I. V. Samarasekera. The Formation of Panel Cracks in Steel Ingots: A State-of-the-Art Review ISS Transactions; volume seven. 1986 - 7.
6. GB 5310-2008 seamless steel tube for high pressure boiler, issued by People's Republic of China national standard in October 2008.
7. F. de Angelis, "A comparative analysis of linear and nonlinear kinematic hardening rules in computational elastoplasticity," Technische Mechanik, vol. 32, no. 2, pp. 164–173, 2012.
8. F. De Angelis and R. Taylor, "Numerical algorithms for plasticity models with nonlinear kinematic hardening," in Proceedings of the 11th World Congress on Computational Mechanics (WCCM '14), Barcelona, Spain, July 2014
9. DL/T 438 thermal power plant metal technology supervision regulation, People's Republic of China electric power industry standard, released in 2009
10. K Garyc, B. Smetana, M. Tkadleckova, et al. Determination of solidus and liquidus temperatures for s34mnv steel grade by thermal analysis and calculations. Metalurgija . 2014, Vol. 53 Issue 3, p295-298
11. R. Zhou, H. Zhang, L. Tang, et al., Xi'an Thermal Power Research Institute Co technical report (number: TPRI/TN-RB-126-2008), 2008, pp34-36.
12. S. H. Ryu and J. Yu, Metall. And Mat. Trans. A, Vol. 29A, p. 1573, June1998.
13. J. N. DuPont. Microstructural Development and Solidification Cracking Susceptibility of a Stabilized Stainless Steel. Welding Research Supplement | 257-s